Seismic event identification

Dale N. Anderson,[1]* George E. Randall,[1] Rodney W. Whitaker,[1]
Stephen J. Arrowsmith,[1] Marie D. Arrowsmith,[1] Deborah K. Fagan,[1]
Steven R. Taylor,[2] Neil D. Selby,[3] Frederick R. Schult,[4]
Gordon D. Kraft,[5] and William R. Walter[6]

Earthquakes and explosions generate seismic waveforms that have different characteristics. However, the challenge of confidently differentiating between these two signatures is complex, and requires the integration of physical and statistical techniques. This article reviews the methods for constructing discrimination features from diverse physical observations. These discrimination features are appropriate for many statistical classification frameworks. Under the null hypothesis an event is an explosion, we discuss strategies for constructing *P*-values which can be interpreted as standardized discrimination features. We develop standardized discriminants for both teleseismic (simple propagation path in the mantle) and regional (complicated propagation path in the crust) events, following the trend toward characterizing increasingly smaller single-point explosions. © 2010 John Wiley & Sons, Inc. *WIREs Comp Stat* 2010 2 414–432 DOI: 10.1002/wics.105

Between 1945 and 1996, the United States (USA), the Union of Soviet Socialist Republics (USSR), the United Kingdom (UK), France, and China executed a total of 2398 nuclear weapon explosions (see Ref 1), including the *Little Boy* and *Fat Man* bombs used by the USA in World War II to force Japan to surrender. The US test *Baker* was detonated in 1946 near the Bikini atoll 27.5 m in the ocean and was observed at seismic stations around the globe. This and other subsequent tests provided scientific evidence that underground nuclear explosions could be detected and potentially characterized with global seismic stations. In the context of nuclear weapon test monitoring, one of the most seismically significant series of tests was executed in 1956 by the UK at the temporary Maralinga test site in Australia. The 1956 Maralinga experiments were by design dual use. In addition to nuclear weapon development data

provided by successful detonation, these experiments provided significant scientific characterization of the Western Australian crust, and amplified the call for seismic research relevant to nuclear weapon test monitoring. The 1957 US experiment *Ranier* was the first fully underground nuclear explosion. *Ranier* was detected by about 50 seismic stations around the globe; however, it was confused with earthquakes at some stations.[2] Discussions on a comprehensive ban of nuclear weapon testing, with participation from the US, UK, USSR, France, Canada, Czechoslovakia, Romania, and Poland, occurred over the summer of 1958 in Geneva. These discussions, fundamentally about eliminating the development of nuclear arsenals through a ban on test explosions, were also motivated by concerns of radioactive fallout because most nuclear explosion tests up to that time were aboveground. A key finding from these discussions was the need for a global network of state-of-the-art seismic stations (specifically arrays) and associated scientific research leading to the operational capability to monitor underground nuclear explosions (see Refs 2 and 3). The 1958 Geneva conference also offered a cautiously optimistic conclusion that techniques to identify seismic events could be developed. In 1961, US deployment of stations comprising the WorldWide Standardized Seismographic Network (WWSSN) began, and by 1966 112 stations were reported operational. This deployment was one

*Correspondence to: dand@lanl.gov

[1]Earth & Environmental Sciences, Los Alamos National Laboratory, PO Box 1663, MS F665, Los Alamos, NM 87545, USA

[2]Rocky Mountain Geophysics, Inc., Los Alamos, NM, USA

[3]AWE Blacknest Seismology Centre, Brimpton, Reading RG7 4RS, UK

[4]Air Force Research Laboratory, Hanscom AFB, MA, USA

[5]Quantum Technology Sciences, Cocoa Beach, FL, USA

[6]Lawrence Livermore National Laboratory, Livermore, CA, USA

component of the US Advanced Research Projects Agency (ARPA) project code named Vela. Project Vela had three main sub-projects; code name Uniform for research and development (R&D) to monitor underground explosions, code name Sierra for R&D to monitor aboveground explosions and code name Hotel for R&D to develop satellite detection systems (see Ref 4 for a contemporary review of project Vela Uniform). Vela was funded to enable the verification of the Partial Test Ban Treaty prohibiting underwater, atmospheric, and outer space nuclear explosion testing. In addition, Vela provided advanced R&D to enable subsequent treaties. A wealth of scientific discoveries on the structure of the earth resulted from WWSSN seismic observations (see Ref 5 for one of many contemporary studies made possible by the WWSSN). Deployment of the WWSSN was a significant first step in real-time seismic monitoring for underground nuclear explosions. The WWSSN offered a wealth of seismic data requiring the development of significant computational efficiencies to estimate the frequency and phase characteristics of seismic waveforms—contemporaneously the fast Fourier transform (FFT) algorithm was developed by Cooley and Tukey.[6] The science of seismology made transformational advances from 1960 through 1980 as a result of seismic monitoring for nuclear explosions, and monitoring research continues to enable significant scientific discovery.

Seismic monitoring for underground explosions answers three questions: Where is the seismic event located? What is the source type (explosion or natural) of the event? How large is the event? Under the Threshold Test Ban Treaty (TTBT), strong seismic waves with a propagation path largely in the mantle (teleseismic waves) were analyzed to answer these questions. Source type identification (discrimination) in seismology is unique in that it focuses on the construction of seismic identification features from seismic waveforms and other multi-technology signatures. Most if not all statistical classification research begins with the assumption 'suppose we have classification features in hand'. In contrast, in seismic identification research, significant effort is directed toward the intelligent construction of the identification features, and how to couple to the features most of the associated and relevant sources of error. These seismic identification features (discriminants) are dynamically adaptable to the number of stations observing an event, the configuration (e.g., geometry) of the observing stations, and the strength of signal at each station. Conceptually, the features are scientifically and statistically constructed to be *evidence quality* in the sense of the *Daubert Standard* before

they are ever combined with a statistical classification method. The Daubert Standard [Daubert v. Merrell Dow Pharmaceuticals, 509 U.S. 579 (1993); General Electric Co. v. Joiner, 522 U.S. 136 (1997); Kumho Tire Co. v. Carmichael, 526 U.S. 137 (1999)] is a collection of United States Supreme Court rulings that in part establishes the requirements for the introduction of scientific analysis as legal evidence in court proceedings. These standards are also applicable and relevant to treaty verification. In summary the Daubert Standard includes five key criteria;

- Has the scientific theory/method been empirically validated?
- Has the scientific theory/method been subjected to anonymous peer review through publication?
- What are the known and potential sources of error when applying the scientific theory/method?
- Are procedures in place to ensure quality and consistency when applying the scientific theory/method?
- Can the scientific theory/method and associated application results be explained with clarity and simplicity?

This article presents the construction of teleseismic and regional (seismic waves with crustal paths) discriminants and two additional multi-technology discriminants derived from infrasonic wave measurements. Coupled with researched sources-of-error models for each discriminant, a general strategy for the construction of diverse multi-technology discriminants has been developed in Refs 7 and 8. This article reviews these developments, including some new extensions, and demonstrates each with open data. The individual discriminants are illustrated with seismic event data acquired from the International Seismological Centre (ISC), the AWE Blacknest Seismological Centre (BSC), Lawrence Livermore National Laboratory (LLNL), and Los Alamos National Laboratory (LANL). These data are available upon request.

For each discriminant a probability model is formulated under a general null hypothesis of H_0 : *Explosion Characteristics*. The veracity of the hypothesized model for each discriminant is measured with a calculation that is exactly, or analogous, to a *P*-value. The hypothesis test formulation ensures that seismic phenomenology is tied to the interpretation of the *P*-value. Most important, the hypothesis test formulation ensures that the physical basis of a discriminant is properly integrated into a probability

model that describes the most relevant source of error corrupting the physical basis measurement. Discriminant *P*-values can also be viewed as standardized discriminants, and can be combined to a unified source type identification with a number of statistical classification methods. Making the null hypothesis H_0 : *Explosion Characteristics* is also important in the context of treaty verification because seismic events are assumed to be single-point explosions and then inferential evidence, as presented in this paper, is used to reject this hypothesis, if possible.

The teleseismic (seismic waves that travel through the mantle) events acquired from the ISC and BSC included nuclear explosions from the Nevada Test Site (NTS) and the former Soviet Union, global earthquakes, and mining explosions from 1964 to 2000. Necessary signal processing was completed by Rocky Mountain Geophysics (RMG). Seismic measurements from combinations of stations given in Table 1 were used in our analysis to demonstrate teleseismic discriminants. LLNL and LANL regional (crustal seismic waves) seismic data included western US earthquakes and Nevada Test Site nuclear explosions. Events were observed with combinations of four seismic stations: Kanab, Utah (KNB, Lat: 37.02, Lon: −112.82); Elko, Nevada (ELK, Lat: 40.75, Lon: −115.24), Landers, California (LAC Lat: 34.39, Lon: −116.41) and Columbia College, California (CMB Lat: 38.03, Lon: −120.39). Regional infrasound data included western US earthquakes and Nevada Test Site nuclear explosions observed by the St. George, Utah (SG, Lat: 37.10, Lon: −113.58) infrasound station. Source type definitions for these data are deep earthquake (DEQ) for a reported depth greater than 50 km, shallow earthquake (SEQ) for a reported depth less than or equal to 50 km, single-point fully contained explosions (EX) and ripple-fire mining explosions (MEX). The number of observed discriminants varies from event to event in those data, and this is typical in seismic event identification analysis. The EX population included underground nuclear weapon tests and some single-point fully contained chemical explosions. Acquired data are summarized by waveform path and source type in Table 2. Figures 1 and 2 show the event and station locations.

TELESEISMIC DISCRIMINANTS

Teleseismic discrimination between underground nuclear explosions and naturally occurring earthquakes has been summarized in a number of publications[9,10] and revisited in Ref 11. The choice of teleseismic discriminants was in part dictated by the seismic data available. The predominant seismic

TABLE 1 | Teleseismic Arrays and Locations

| Station	Latitude	Longitude	Description
CLL	51.31	13.00	Collm, Germany
EKA	55.33	−3.16	Eskdalemuir Array, Scotland
GBA	13.60	77.44	Gauribidanur Array, India
HFS	60.13	13.70	Hagfors Array, Sweden
INK	68.31	−133.52	Inuvik, Northwest Territories, Canada
KHC	49.13	13.58	Kasperske Hory, Czech Republic
KIR	67.84	20.42	Kiruna, Sweden
LOR	47.27	3.86	Lormes, France
MBC	76.24	−119.36	Mould Bay, Northwest Territories, Canada
NDI	28.68	77.22	New Delhi, India
NUR	60.51	24.65	Nurmijarvi, Finland
SSF	47.06	3.51	Saint Saulge, France
UME	63.82	20.24	Umea, Sweden
UPP	59.86	17.63	Uppsala Sweden
WRA	−19.94	134.34	Warramunga Array, Australia
YKA	62.49	−114.61	Yellowknife Array, Canada

Arrays EKA, GBA, WRA and YKA comprise the United Kingdom seismic system.

TABLE 2 | Source Type Summary by Waveform Path

Waveform Path	EX	SEQ	DEQ	MEX
Teleseismic	395	452	144	30
Regional/Infrasound	163	73	NA	0

systems were, by current standards, relatively narrow band sensors with limited dynamic range recording systems. The typical pairing of long-period sensors (centered at about 20 s period) and short period sensors (centered at about 1 s period) was well designed to minimize the effect of the ambient microseismic noise centered at about a 6-s period.

A seismic event couples energy into the earth, and this energy is partitioned into waveform phases (segments). The path and distance between event and stations are different and if the phase energy measurements from each station could be reasonably corrected for these effects, the measurements would be quite similar, with differences fundamentally due to near-source and near-station effects. Magnitudes are empirical measurements of phase energy in logarithmic units that include corrections for these effects. Significant research on correction models includes Refs 12–14. Station magnitudes are modeled
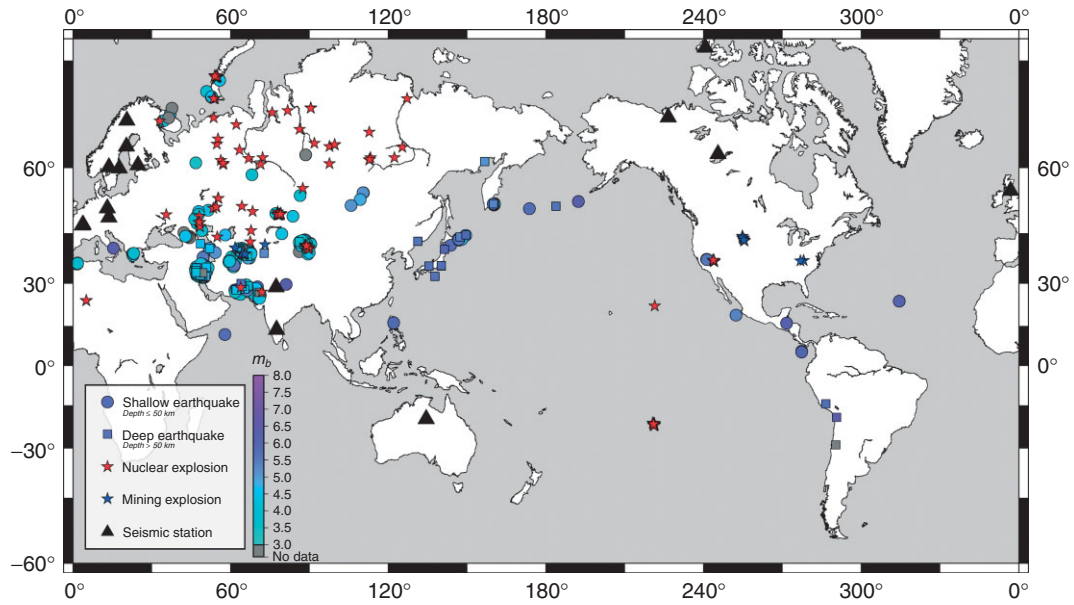
FIGURE 1 | Teleseismic event and station locations.
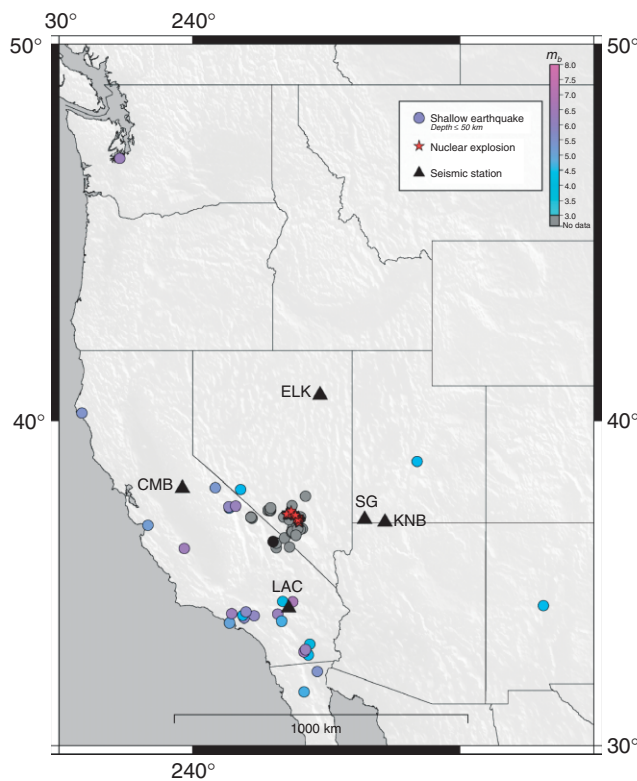
FIGURE 2 | Regional event and station locations.

as Gaussian and are combined (e.g., averaging) to estimate an event network magnitude. For each station in a network, common magnitudes used for event identification are the body-wave magnitude (m_b) and surface-wave magnitude (M_S) computed from windows in the primary (P) and Rayleigh (R) waveform segments, respectively (see Figure 3). Regional distance (approximately 300–2000 km) discrimination makes use of P and secondary (S) waveform segments.
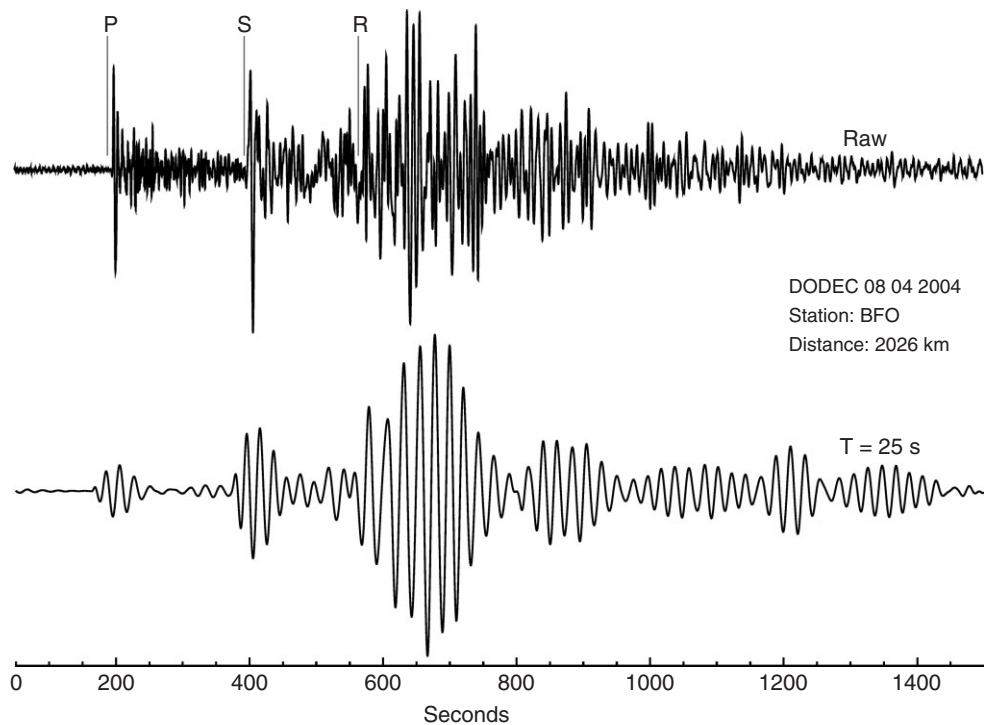
FIGURE 3 | P, S, and Rayleigh (R) phases for a seismic waveform, both as raw data (top) and filtered (bottom) at 25 s. Information about the event, and about M_S measurement can be found in Ref 15.

The typical magnitudes from earthquake seismology were calibrated for m_b using the short period sensor and M_S using the long period sensor. The relatively young science of seismology had grown using the observables from these paired sensors. Event magnitude, the first motion of the vertical component, location based on observed arrival times, and depth phases indicating event depth were all classical seismological tools built to study earthquakes. The differences in observations for underground nuclear explosions lead to the development of teleseismic event discrimination. Clearly documented depth phases implied event depths far too deep to have been nuclear explosions. First motions that showed a clear radiation pattern of up and down first motions were inconsistent with the pure explosion source. The comparison of m_b and M_S magnitudes showed difference between naturally occurring earthquakes and underground nuclear explosions. Teleseismic event discrimination survives today, now using modern broad band seismic sensors and high dynamic range digital telemetry and recording systems. The data can be digitally filtered to emulate the earlier measurements, and consistent results can be generated. Skilled analysts now use digital computers and algorithms to take measurements using computer displays, but the measurements are still fundamentally the same as those by early analysts for analog recordings on paper or photographic recordings. The success of teleseismic discrimination is limited only by the signal-to-noise ratio for small

seismic events and the global distribution of seismic stations. The success of teleseismic discrimination is a tribute to the early researchers in the field who developed sophisticated yet simple discriminants.

Depth from Hypocenter Estimation

The physical basis for event depth as a discriminant is simple—single-point underground explosions can only be detonated at a depth of less than drilling capability. In contrast, natural seismicity can extend to many hundreds of kilometers depth. From a mathematical statistics perspective hypocenter (epicenter and depth) estimation is nonlinear regression (see Ref 16). A set of well-associated seismograms (seismograms generated by the same seismic event) gives a set of P-phase arrival times (teleseismic and/or regional) for an event. Let t_0 denote the origin time of the seismic disturbance and let t_i denote the arrival time of the P-wave at seismometer i. Let $\underline{S}_0 = (x_0, y_0, z_0)'$ (epicenter and depth) be the location of the seismic event and $\underline{S}_i$ be the location of seismometer i. Estimates of the unknown quantities t_0 and $\underline{S}_0$ are desired. Theoretical travel time $T(\underline{S}_i, \underline{S}_0)$ as a function of the distance between a seismic disturbance $\underline{S}_0$ and a seismometer $\underline{S}_i$ has been tabulated for use in all aspects of seismic monitoring. With this travel-time function

$$(t_i - t_0) = T(\underline{S}_i, \underline{S}_0) + \epsilon, \tag{1}$$

where the error terms ϵ, in general, are multivariate Gaussian.

The hypotheses are $H_0 : z_0 \leq z_0'$ and $H_A: z_0 > z_0'$. Define the nonlinear least squares function

$$SSE(\underline{S}_0, t_0) = \sum_{i=1}^{n} \left(t_i - t_0 - T(\underline{S}_i, \underline{S}_0)\right)^2. \quad (2)$$

Allowing all parameters $\underline{S}_0$ and t_0 to float freely when minimizing $SSE(\underline{S}_0, t_0)$ gives the minimum value $SSE(\hat{\underline{S}}_0, \hat{t}_0)$. If depth is constrained to be $z_0 = z_0'$, then the minimum sum of squared residuals is $SSE(\hat{\underline{S}}_0, \hat{t}_0 \mid z_0 = z_0')$. Under H_0, the statistic

$$F_{1,n-4} = \frac{SSE(\hat{\underline{S}}_0, \hat{t}_0 \mid z_0 = z_0') - SSE(\hat{\underline{S}}_0, \hat{t}_0)}{SSE(\hat{\underline{S}}_0, \hat{t}_0)/(n-4)} \quad (3)$$

has an approximate central F-distribution with $1, n - 4$ degrees of freedom, and

$$T_{n-4} = \text{sign}(\hat{z}_0 - z_0')\sqrt{F_{1,n-4}} \quad (4)$$

has an approximate central Student's T-distribution with $n - 4$ degrees of freedom, which provides a P-value.

$H_0 : z_0 \leq 50$ P-values are shown in Figure 4. The interpretation of the depth P-value as evidence in support of $H_0 : z_0 \leq 50$ leads to no missed explosions. Treating the P-value as a standardized discriminant, and choosing a classification decision line of approximately 0.2 also leads to no missed explosions with a significant reduction events of concern.

Body- versus Surface-wave Magnitudes

The m_b versus M_S discriminant is based on empirical observations that shallow earthquakes generally have a higher M_S than a single-point fully contained explosion with the same m_b. The m_b versus M_S discriminant is quite mature (see Refs 17–20). The competing hypotheses are $H_0 : \mu_{m_b} - \mu_{M_S} \geq \Delta_0$ and $H_A: \mu_{m_b} - \mu_{M_S} < \Delta_0$. The discriminant is formed from the difference of network averaged surface- and body-wave magnitudes $\tilde{m}_b$ and $\tilde{M}_S$. Subtracting the historical average of this difference, when the seismic source is an explosion, and then dividing by the standard error gives a standardized difference. The common variance (σ^2) for m_b and M_S in the standard error is calculated from historical data and is assumed known. Specifically, a common formulation is

$$Z = \frac{(\tilde{m}_b - \tilde{M}_S) - \Delta_0}{\sigma\sqrt{1/n_{\tilde{m}_b} + 1/n_{\tilde{M}_S}}}. \quad (5)$$

However, other established formulations use $(\tilde{m}_b - c\tilde{M}_S)$ as the numerator with c derived from calibration data.

The standard error in Eq. (5) is inconsistent with physical basis in that an event observed by a large number of stations will have an unrealistically small standard error. Conceptually this implies that the path and distance corrections for the magnitudes m_b and M_S are accurately known and applied, and these magnitudes are corrupted only by incoherent (uncorrelated) station noise. However, physical path and distance corrections are specific to an event and realistically can only be approximately modeled. If correction model inadequacy (e.g., variations in attenuation) is treated as random then with historical event

FIGURE 4 | P-values for the hypothesis H_0 : event depth ≤ 50 km. The abscissa is the established seismic catalog event depth. Single-point fully contained explosions are shown in red, shallow earthquakes are yellow, deep earthquakes are green, and mining explosions are gray.
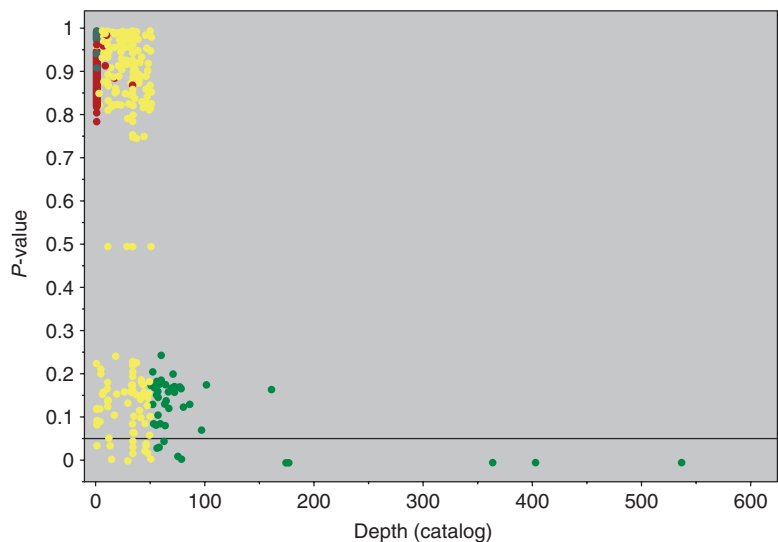
data the variance components for correction model error and station noise can be estimated. The conceptual formulation of the random effects model for a magnitude is

$$Y = Magnitude = \mu(source - type) + Event + Noise \tag{6}$$

where *Event* is a random effect that varies from event to event and represents model inadequacy in physical path and distance corrections. *Noise* represents measurement and station noise. The value Δ_0 in Eq. (5) is calculated from calibrated values of $\mu(source - type)$ for the magnitudes m_b and M_S.

Define the random variable Y_{ijk} to be a magnitude for source-type $i = 0, 1$ (SEQ, EX), event j and station k (observed data are denoted y_{ijk}). The linear model representation of Eq. (6) is then

$$Y_{ijk} = \mu_i + E_j + \epsilon_{(ij)k}; \qquad j = 1, 2, \ldots m_i, \quad k = 1, 2, \ldots, n_{ij}. \tag{7}$$

Equation (7) reads Y_{ijk} equals a constant source-type mean μ_i plus a random event adjustment E_j (model inadequacy) plus a station noise adjustment $\epsilon_{(ij)k}$. The E_j are iid normal random variables with zero mean and variance τ^2. The $\epsilon_{(ij)k}$ are iid normal random variables with zero mean and variance σ^2. E_j and $\epsilon_{(ij)k}$ are independent across all subscripts. This assumption is consistent with near-source and path effects being uncorrelated with station noise. The intra-class correlation $(\tau^2/(\tau^2 + \sigma^2))$ has an important interpretation. It implies that large adjustment E_j increases correlation between stations because a significant part of this random effect comes from near-source effects applied to all stations observing an event. Small adjustment E_j implies the correction model is good and is conceptually equivalent to error structure from stations with incoherent noise. Small adjustment E_j implies τ^2 is small and the standard error of $\bar{Y}_{ij}$ is reduced further through station averaging.

From the model Eq. (7), the standard error of the m_b versus M_S discriminant is

$$SE_{\tilde{m}_b - \tilde{M}_S} = \sqrt{\tau_{m_b}^2 + \frac{\sigma_{m_b}^2}{n_{m_b}} + \tau_{M_S}^2 + \frac{\sigma_{M_S}^2}{n_{M_S}}} \tag{8}$$

for both earthquakes and explosions and the test statistic is

$$Z = \frac{(\tilde{m}_b - \tilde{M}_S) - \Delta_0}{\sqrt{\tau_{m_b}^2 + \frac{\sigma_{m_b}^2}{n_{m_b}} + \tau_{M_S}^2 + \frac{\sigma_{M_S}^2}{n_{M_S}}}}, \tag{9}$$

providing a *P*-value for the hypothesis test $H_0 : \tilde{m}_b - \tilde{M}_S \geq \Delta_0$. We note that this extended formulation of the m_b versus M_S discriminant is analogous to the formulation of regional amplitude discriminants in Ref 8 and reviewed below.

In addition to observed discrimination properties, both m_b and M_S are biased proxy measurements for the size of an event—seismic moment([=] Newton/meter) for earthquakes and yield ([=] kilotons TNT) for explosions. The network magnitudes $\tilde{m}_b$ and $\tilde{M}_S$ are biased measurements for event size with increased precision. For earthquakes, we propose that this bias is significantly due to inadequate correction for event depth, the radiation pattern of the earthquake (fault orientation) and near-source earth structure, which in the aggregate we model as the random correction model error E_j. For explosions, this bias is significantly due to inadequate correction for event depth, the radiation pattern from tectonic release caused by the explosion and near-source earth structure, also modeled in the aggregate as random correction model error E_j.

Applying (apparent performance) the discriminant formulation Eq. (9) to the ISC/BSC teleseismic data gave $\Delta_0 = 1.35$, $\tau_{m_b}^2 = 0.24$, $\tau_{M_S}^2 = 0.56$, $\sigma_{m_b}^2 = 0.15$ and $\sigma_{M_S}^2 = 0.14$. *P*-values are shown in Figure 5. Deep earthquakes (DEQ) can attenuate the waves that generate the magnitude M_S and so DEQ events can appear to be single-point explosions. In this case, resolution requires the depth discriminant developed above to eliminate the deeper earthquakes. The combination of the depth and m_b versus M_S discriminants is shown in Figure 6. Note that an interpretation of the m_b versus M_S *P*-value as evidence in support of $H_0 : \tilde{m}_b - \tilde{M}_S \geq 1.35$ leads to no missed explosions. Treating the *P*-value as a standardized discriminant, and choosing a decision line of approximately 0.2 also leads to no missed explosions with a significant reduction in false-alarms.

Observed Depth Phases

A depth estimate can be obtained from the difference in arrival times of the compressional P and pP phases. A schematic example is illustrated in Figure 7. The P-wave travels directly from a seismic disturbance to a seismometer. In contrast, the pP-wave is a reflected P-wave traveling from the seismic disturbance to the earth's surface before being reflected to the same seismometer. The time difference between the arrival of P- and pP-phases, $\delta t_{pP} = t_{pP} - t_P$, is a function of the depth of the seismic source and the epicentral distance from the source to the seismometer. The relationship between the depth of the seismic focus, epicentral

FIGURE 5 | P-values for H_0 : $\mu_{m_b} - \mu_{M_S} \geq 1.35$. The abscissa is the average epicentral distance (degrees) between event and seismic stations. Single-point fully contained explosions are shown in red, shallow earthquakes are yellow, and deep earthquakes are green.
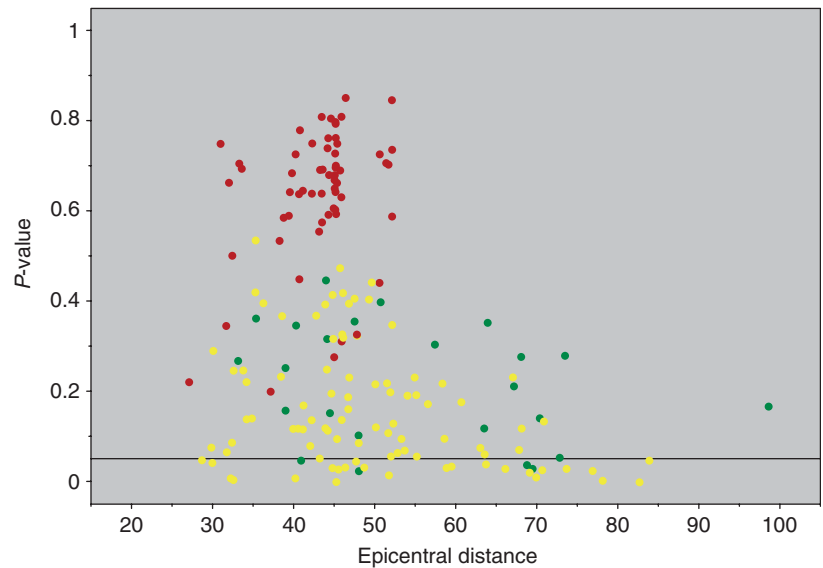
FIGURE 6 | Bivariate plot of m_b versus M_S (mb/Ms) and depth P-values. Single-point fully contained explosions are shown in red, shallow earthquakes are yellow, and deep earthquakes are green.
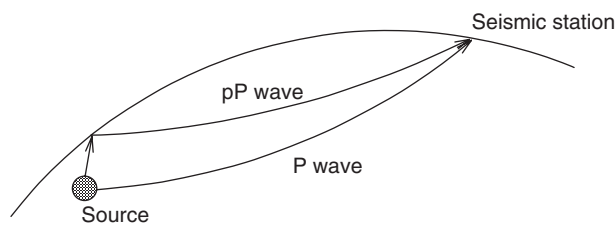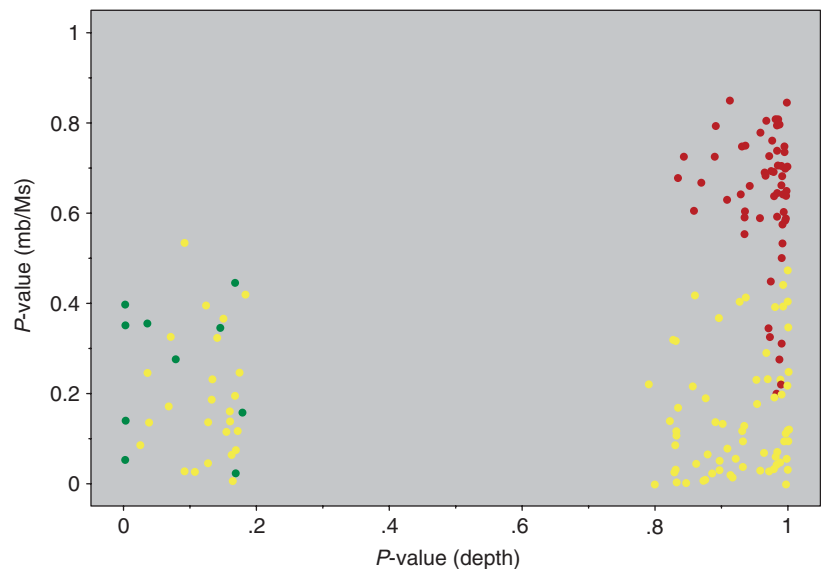

FIGURE 7 | The direct P phase and the surface reflected pP phase are shown as ray paths.

distance, and δt_{pP} is given in the International Association of Seismology and the Physics of the Earth's Interior (IASPEI) tables.[21,22]. δt_{pP} is predominantly dependent on the depth of a seismic event when the focus is less than approximately 100 km deep. Given

δt_{pP} from even a single seismometer and an epicenter estimate, a depth estimate can be obtained. However, any such estimate must be taken with caution since identification of reflected waves generally requires the presence of candidate pP-waves at several stations to establish that the waves are, in fact, reflected waves. A key feature that one looks for in this situation is how well the candidate waves fit the stepout for pP. Generally, stepout is the change in the time differences, δt_{pP}, as a function of epicentral distance. Observed high-quality station pP phase arrivals from a deep event will have a predictable relationship between δt_{pP} and distance. Plots of δt_{pP} versus epicentral distance Δ between station and event are shown in Figure 8.

Transforming with logarithms improves linearity (Figure 8 right), especially for deep events. For
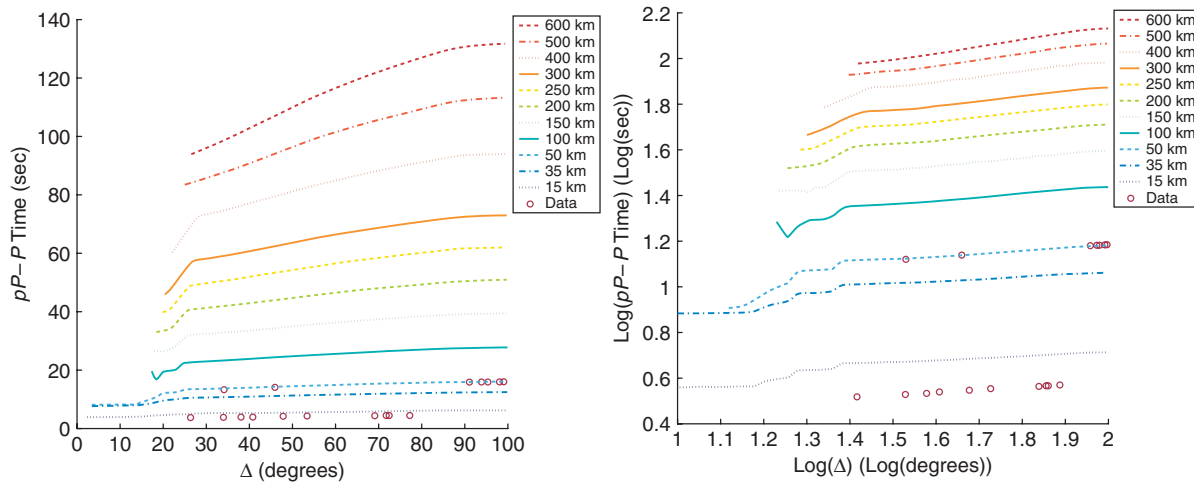
FIGURE 8 | IASPEI travel time curves for $pP - P$ are shown in raw form (left) and in the log domain (right) for a series of different event depths. Superimposed on the curves are data for 10- and 50-km-deep events.

teleseismic data (greater than $20°$ epicentral distance), the curves are quite linear. It should be noted that pP phases are very difficult to identify at regional distances (less than $20°$ epicentral distance) because the pP onset times are mixed with crustal seismic waves. Thus pP is primarily used as a discriminant for stations between 20 and $100°$ epicentral distance. Shown on the plots of Figure 8 are data from two well-behaved events, 10- and 50-km deep. When the data are fit with a linear regression model, both the slope and intercept increase with event depth. For the shallower depths, the slopes are quite small. The error associated with slope is much larger than the error associated with intercept. It is quite obvious that a pP discriminant should take into account the number of pP phases as well as an indication of strength of evidence that the phases are truly pP. This can be accomplished with regression analysis (see Ref 23) to obtain the slope, intercept and errors for stepout versus Δt. The regression analysis should include outlier removal to adjust to poor phase arrival picks.

For station i, the simple linear regression (SLR) model for δt_{pP_i} and Δ_i is

$$\ln\left(\delta t_{pP_i}\right) = \beta_0 + \beta_1 \ln\left(\Delta_i/\tilde{\Delta}\right) + \epsilon_i \qquad (10)$$

where $\tilde{\Delta}$ is the geometric average of the epicentral distances between stations $i = 1, 2, \ldots, n$, and event and ϵ_i are independent and identical normal random variables with mean zero and constant variance σ^2. The SLR estimates of β_0 and β_1 are statistically independent with this formulation. $\beta_0 = \log\left(\delta t_{pP_i}\right)$ at the distance $\Delta_i = \tilde{\Delta}$ and so β_0 has a direct

relationship to event depth z_0 at this distance—if β_0 is relatively large then significant depth is indicated.

The composite null hypothesis is $H_0 : \beta_0 \leq b_0$ and $\beta_1 \leq b_1$. The b_0 and b_1 values are determined from minimum depth natural events with clearly observable stepout and P-wave surface reflections. The test statistics are

$$T_{\beta_j, n-2} = \frac{\hat{\beta}_j - b_j}{SE_{\hat{\beta}_j}} \quad j = 0, 1 \qquad (11)$$

where $SE_{\hat{\beta}_j}$ is the standard error of the regression estimate $\hat{\beta}_j$. $T_{\beta_j, n-2}$ follows a Student's T-distribution with $n - 2$ degrees of freedom providing P-values for both tests. b_0 speaks to depth and b_1 speaks to strong stepout. If $H_0 : \beta_0 \leq b_0$ and $\beta_1 \leq b_1$ is true then p_{β_0} and p_{β_1} are independent uniform random variables and $\chi^2 = -2\ln(p_{\beta_0}) - 2\ln(p_{\beta_1})$ is a chi-squared random variable with 4 degrees of freedom providing a P-value for the composite null hypothesis.

An alternate formulation can be based on order statistics (OS)—it requires that statistics theory adapts to physical basis. The OS formulation of the discriminant is a compound probability distribution of two measurements—the number of observed depth phases (number of observed pP) from an event, and a measurement of stepout. The formulation that follows closely resembles an expert rule-based formulation. The physical basis of the two measurements, the number of observed depth phases and stepout, are integrated into a H_0 probability model. The P-value is then calculated as a measurement of agreement with this probability model. In combination, the two measurements can indicate high confidence in the
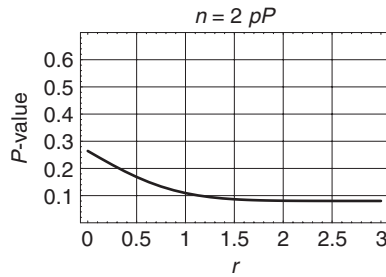
FIGURE 9 | Order statistic pP discriminant P-value as a function of $R = r$ stepout in seconds for $n = 2$ observed pP.

observation of depth phases. The null hypothesis is conceptual—H_0 : No observed pP. As with the SLR formulation, inconsistency with H_0 is indicated when the number of observed pP is large or observed stepout is large. As will be demonstrated, the OS formulation will give a small P-value when good-quality depth phases are seen; however, solid inconsistency with H_0 additionally requires observed stepout. For example, the formulation provides solid inconsistency with H_0 with only two observed pP and strong stepout. In contrast, many observed pP with weak stepout indicates only marginal inconsistency with H_0. This is illustrated in Figure 9 for $n = 2$ observed pP.

The joint probability model of stepout and number of observed pP phases is developed as the product of two component probabilities $Pr(N = i) \times Pr(R \leq r|N = i)$, where

- N is the number of observed pP and
- R equals the difference between δt_{pP} from the farthest station and δt_{pP} from the closest station.

Note that the calculation of R is, for all practical purposes, equal to $Max(\delta t_{pP}) - Min(\delta t_{pP})$ and is assumed to be so in the following development. For very shallow events, or poorly associated events, R can be negative—in these cases it is set equal to zero. Under H_0 the number of observed pP will be zero or extremely small (from spurious picks). A probability model often used for rare events is the Poisson distribution

$$Pr(N = i) = \frac{\eta^i e^{-\eta}}{i!}; \quad i = 1, 2, \ldots \quad (12)$$

Here η is conceptually the expected number of spurious pP picks from a large number of event waveforms. Under H_0 the distribution of the δt_{pP} from an event are modeled with the cumulative distribution function (CDF) $\Phi(\cdot)$ and probability density function

(PDF) $\phi(\cdot)$. With the assumption that R is equivalent to $Max(\delta t_{pP}) - Min(\delta t_{pP})$, its probability model can be derived as a function of the smallest and largest order statistics, $Max(\delta t_{pP})$ and $Min(\delta t_{pP})$.

$$Pr(R \leq r|N = i) = i \int_{-\infty}^{\infty} (\Phi(v - r) - \Phi(v))^{i-1} \phi(v) dv$$

$$r \geq 0; \quad i = 1, 2, \ldots. \quad (13)$$

A test of the conceptual hypothesis H_0 : No observed pP is essentially inference by contradiction— H_0 is assumed true until it is proved false. With this reasoning, $Pr(R \leq r|N = 0) = 1$ because no observed pP is consistent with H_0. Strong inconsistency with H_0 requires a measure of stepout. With the same reasoning, if only one pP is observed, then again $Pr(R \leq r|N = 1) = 1$. For n observed pP picks and an observed stepout of r, the P-value is then calculated as

$$P\text{-value} = 1 - Pr(N \leq n, R \leq r)$$
$$= 1 - \sum_{i=1}^{n} Pr(N = i) \times Pr(R \leq r|N = i), \quad (14)$$

where $Pr(R \leq r|N = i) = 1$, $i = 0, 1$, and $Pr(R \leq r|N = i) = 0$, $r \leq 0$. The P-value calculation is illustrated graphically in Figure 10.

To apply the two pP discriminant formulations to the ISC/BSC data, model the stepout CDF ($\Phi(\cdot)$)
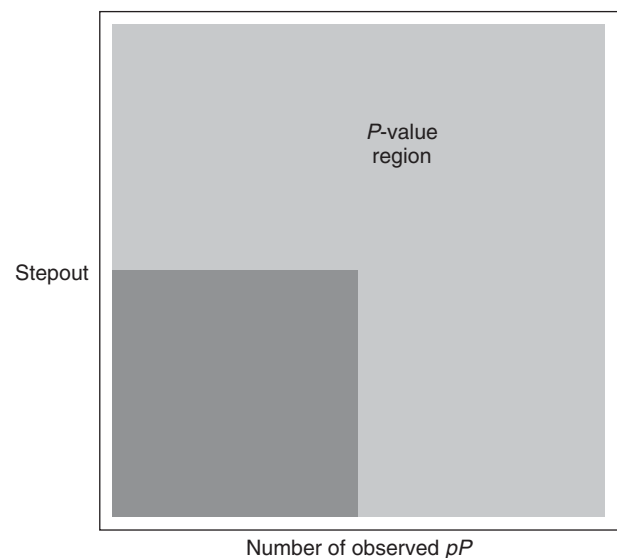
FIGURE 10 | P-value calculation for the order statistic formulation of the pP discriminant. The joint probability model for stepout and number of observed pP is integrated over the dark gray region and subtracted from one, giving the P-value.
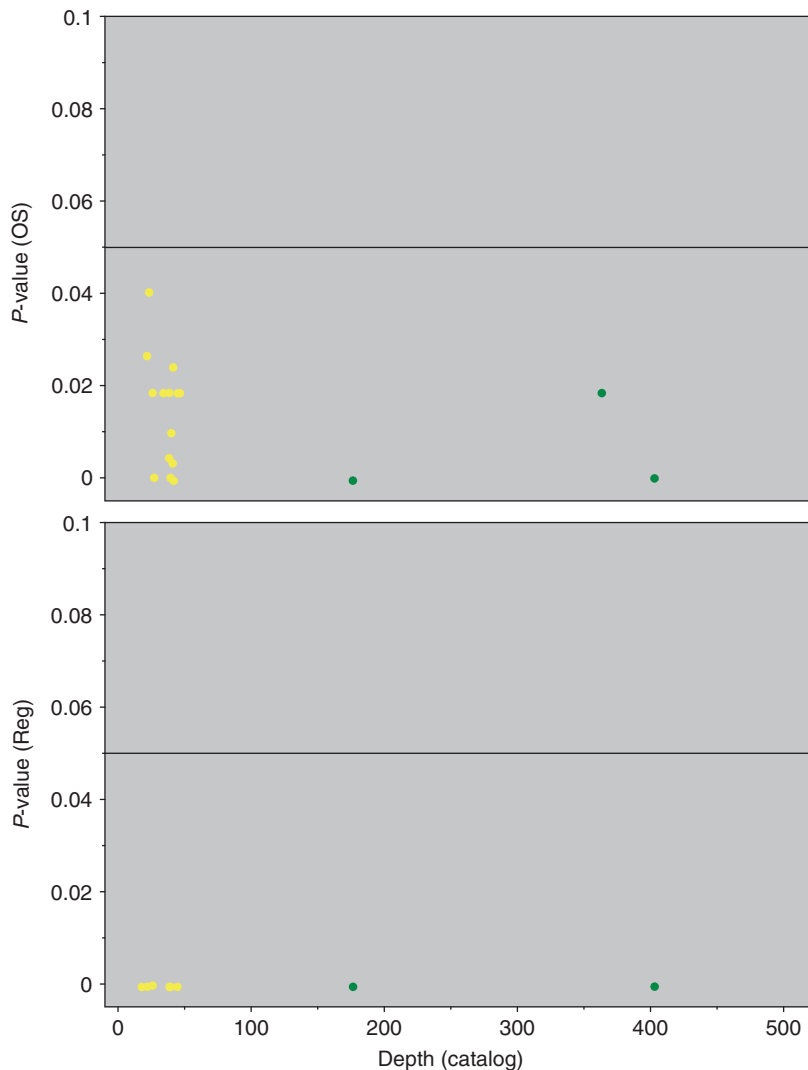
FIGURE 11 | *P*-values for the order statistics and regression formulation of the *pP* discriminant are top and bottom respectively. The abscissa is the average epicentral distance (degrees) between event and seismic stations. Shallow earthquakes are yellow, and deep earthquakes are green.

and PDF ($\phi(\cdot)$) in Eq. (13) as normally distributed with mean 1 and standard deviation 0.5. These values are reasonably consistent with the travel time table of δt_{pP} for depths less than 35 km. The Poisson parameter is modeled with $\eta = 1$. Also consistent with depths less than 35 km, the null hypothesis for the regression formulation is $H_0 : \beta_0 \leq 1$ and $\beta_1 \leq 0$. Because these discriminant formulations are only calculated when an analyst asserts observed *pP* arrivals, they are both essentially deep event rejectors. Figure 11 demonstrates that both discriminants corroborate the ISC/BSC analyst *pP* picks. The regression formulation exhibits consistently stronger evidence to reject the null hypothesis because of the regression intercept and it's direct relationship to event depth. However the advantage of the order statistics formulation is that it enables a *P*-value calculation with only $n = 2$ observed *pP*.

First Motion

Excluding pathological cases, a seismogram from an underground explosion exhibits the initial earth movement as upward or positive, regardless of the location of the seismometer. In contrast, an earthquake is caused by relative movements of adjacent blocks of the earth due to tectonic forces. As a discriminant, if the first motion of a seismic signal in a waveform is negative at some stations, then the seismic disturbance is unlikely to be an explosion. If the first motion is positive at all stations, then the seismic event might be the result of an explosion. The ambiguity under unanimous positive first motion is potentially caused by an inadequate distribution of seismic stations (*e.g.*, no earthquake *P*-waves with negative first-motion polarity travel to areas with seismic network coverage) or poor signal-to-noise ratio (inability to observe the *P*-wave signal because it is too small compared to background noise).

With good signal-to-noise at each station the polarity of first arrival is usually correctly identified; however, it can be mistaken. Uncertainty in identifying first arrival polarity motivates a statistical construction of the discriminant. The null hypothesis is conceptual—H_0: The source mechanism is a single-point fully contained explosion. Under H_0, the probability of positive first motion at a station is composed of two component probabilities: the probability of positive first motion from the source, and the probability that first motion polarity is correctly determined given positive first motion from the source.

The first component equals one under H_0. There may be pathological cases where this is not true; however, they are assumed negligible for this development. The second component probability is governed by many factors including signal-to-noise and analyst training and experience, all influencing an accurate first arrival pick. For this development, with good signal-to-noise at all stations, this probability is modeled as a constant. This reasoning is succinctly summarized as

Pr(+ first motion observed at a station)

$= Pr$(+ first motion from source)

$\times Pr$(first motion polarity correctly identified |

+ first motion from source) $= 1 \times \theta$. (15)

From this formulation, there may or may not be a positive first motion at each station—a binary random variable with Pr(+ first motion observed at a station) $= \theta$. Assume that stations are probabilistically independent. Therefore, for M stations forming an event, the number of stations $(N = n)$ under H_0 that have positive first motion has a binomial distribution with parameters M and θ. For observed $N = n$, the P-value is simply the binomial cumulative distribution function

$$P\text{-value} = \sum_{i=0}^{n} \binom{M}{i} \theta^i (1 - \theta)^{M-i} \quad n = 0, 1, 2, \ldots, N. \quad (16)$$

The parameter Pr(+ first motion observed at a station) $= \theta$ will be nearly one under H_0. However, this discriminant should be excluded from an identification analysis if first motion is identified positive at all stations—the polarity of first motion discriminant is fundamentally an explosion rejector. Events with good signal-to-noise and a sufficient number of stations with negative first motion confidently reject H_0.

Under the null hypothesis H_0, model $\theta = Pr$(+ first motion observed at a station) equal to 0.95. For this parameter value, example plots of the P-value versus $N = n$ are given in Figure 12 for $M = \{6, 7\}$. In Figure 13, the interpretation of the first motion P-value as evidence in support of H_0 leads to an unacceptable number of rejected explosions at the 5% significance level. This is because the first motion

FIGURE 12 | Polarity of first motion discriminant P-value as a function of the number of stations $(N = n)$ that have positive first motion for $M = \{6, 7\}$.
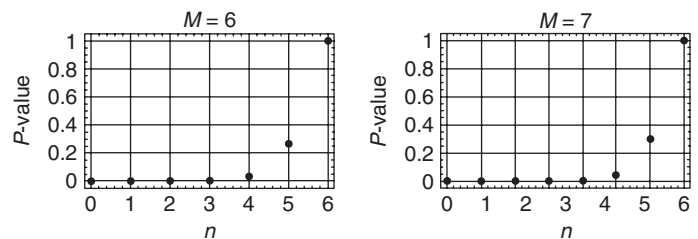
FIGURE 13 | P-values for the first motion hypothesis H_0 : The source mechanism is a single-point fully contained explosion. The abscissa is the network (average) event $\tilde{m}_b$. Single-point fully contained explosions are shown in red, shallow earthquakes are yellow, deep earthquakes are green, and mining explosions are gray.
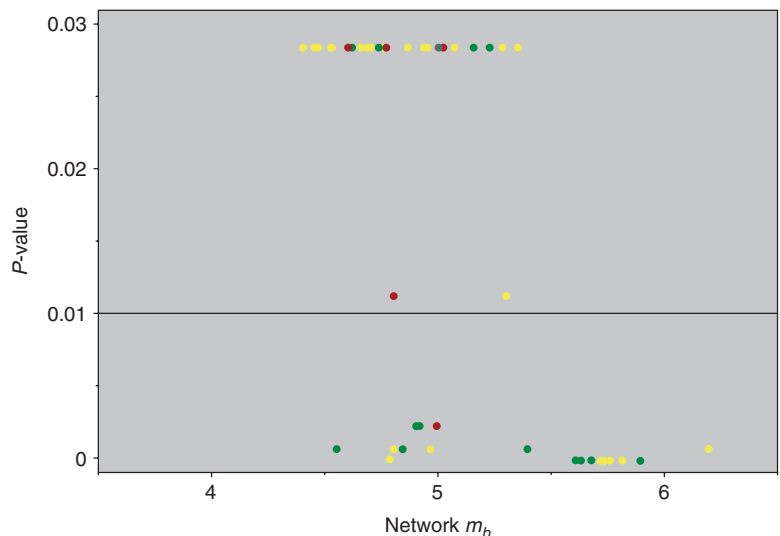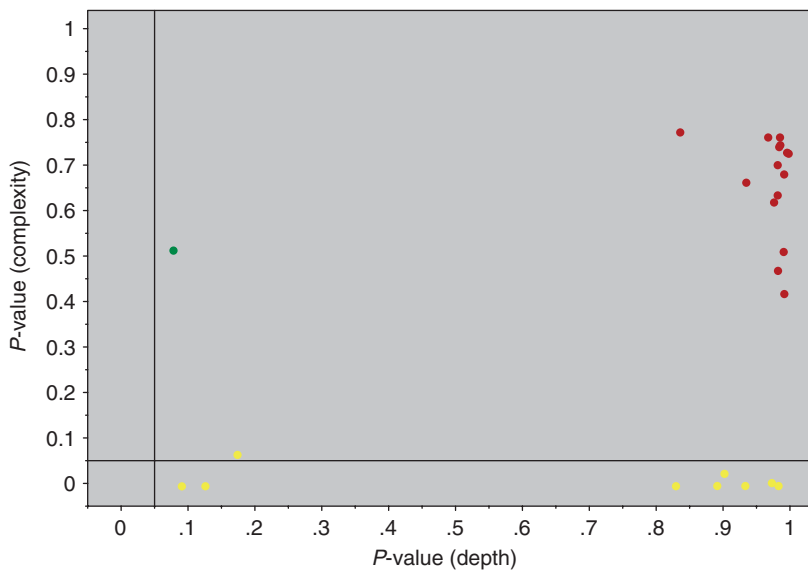
FIGURE 14 | Bivariate plot of complexity and depth P-values. The complexity P-values (typicality indices) are for a multivariate test of the hypothesis H_0 : Station complexity discriminants are from the single-point fully contained explosion population. Explosions are shown in red, shallow earthquakes are yellow, and deep earthquakes are green. Arrays used in the analysis are EKA, GBA, WRA and YKA listed in Table 1.

of stations observing these explosions was likely, and erroneously, identified as negative. Treating the P-value as a standardized discriminant, and choosing a decision line of approximately 0.01 rejects only one explosion however with increased false-alarms.

Waveform Complexity

Taylor and Anderson[24] review the development of the single-array teleseismic complexity discriminant and demonstrate a multivariate discrimination with complexity. Conceptually, shallow earthquakes have complex P-wave signatures relative to single-point fully contained explosions. This is mainly due to the fact that earthquakes can generate complex signals from the rupture process, including reflected depth phases such as pP. Even though complexity measurements, in current application, are specific to an array and path, studies suggests that multi-array (multivariate) complexity measures may be effective for teleseismic event screening and regional discrimination.[25,26] The reasoning is that at certain azimuths and low signal-to-noise ratio, only P or pP may be observed from an earthquake, resulting in an apparent simple waveform. Multivariate complexity measures at different azimuths will mitigate this effect with the inclusion of stations having higher signal-to-noise ratio. Single-point fully contained explosions are usually simple, impulsive point sources. Analogous to the m_b versus M_S discriminant, seismic measures of complexity cannot be used to positively identify an explosion without some indication of depth. This is because of attenuation of energy for deep earthquakes. Significant studies on the physical mechanisms of simple and complex waveforms include Refs 27–30. Also, simulations

indicate that multi-array (multivariate) complexity measurements would reduce false alarm rates.[30]

In the study by Taylor and Anderson,[24] complexity is defined as

$$\beta_C = \log \frac{E_{coda}}{E_{signal}}, \qquad (17)$$

where E_{coda} is the average energy (mean square) of the coda in the 5 to 25 second window after the P-wave arrival time, and E_{signal} is the average signal energy in the 5 second window after the P-wave arrival time. Standard array processing techniques are used to derive E_{coda} and E_{signal}.

Figure 14 shows multi-array complexity P-values from a calibration analysis with arrays EKA, GBA, WRA and YKA. These P-values are in fact typicality indices proposed in Ref 31 for the single-point fully contained explosion population. An interpretation of the complexity P-value as evidence in support of the explosion population leads to no missed explosions. Treating the P-values as standardized discriminants, and choosing a decision line of approximately 0.1 also leads to no missed explosions with no false-alarms. Note also that the depth P-value dismisses the deep earthquake.

REGIONAL DISCRIMINANTS

Regional discrimination between underground nuclear explosions and naturally occurring earthquakes is an evolving field which represents a paradigm shift, driven by a desire to discriminate ever smaller events. The amplitude of smaller events results in weaker signals at teleseismic distances, frequently

buried in the ambient noise. As well as concerns about smaller events, driven by the treaty monitoring, technology for seismic sensors and recorders has improved dramatically, allowing broad band sensors and wide dynamic range digital recording coupled with digital computer analysis tools. The push to regional distances (approximately 300–2000 km) has enabled the recording of much smaller seismic events, but has come at a price of additional seismogram complexity. The shorter propagation path means less amplitude loss from geometrical spreading and attenuation, with higher-frequency information preserved.

The regional distance propagation paths are predominately through the crust and upper mantle of the earth, the most heterogeneous portion of the earth. Regional seismograms can exhibit wide variations in the relative amplitudes of seismic arrivals based on the particular propagation path, but common features persist. Shear energy is generally weaker relative to compressional energy for underground nuclear explosions compared to earthquakes, as is also seen at teleseismic distances for larger events (m_b versus M_S). Difficulty arises because discrimination rules developed for one region need to recalibrated or even revised for another region with significantly different geologic structure. Early work in regional seismic discrimination is summarized in Refs 19 and 32, and remains an active area of research.

Phase Amplitude Discriminants

Analogous to the path and distance corrections for teleseismic magnitudes, Taylor et al.[33–35] develop the Magnitude and Distance Amplitude Correction (MDAC) for regional phase amplitudes (e.g., P_n, P_g,

S_n, L_g). MDAC is a function of frequency and makes regional amplitudes independent of distance, magnitude and station. As with magnitudes, regional amplitudes are in logarithm units. The difference of regional P (e.g., P_n or P_g) and S (e.g., S_n or L_g) wave amplitudes at high frequencies can discriminate between earthquakes and explosions (see Refs 36–38). The sources-of-error model for regional phase amplitude discriminants is developed in Ref 8. Specifically, for P_g versus L_g, both constructed with a 6–8 Hz filter window, the competing hypotheses are $H_0 : \mu_{P_g} - \mu_{L_g} \geq \Delta_0$ and $H_A : \mu_{P_g} - \mu_{L_g} < \Delta_0$. The sources-of-error model formulation for regional phase amplitude discriminants is that of Eq. (7), with Y_{ijk} the corrected amplitude for source-type $i = 0, 1$ (earthquake, explosion). Analogous to the m_b versus M_S discriminant, Eq. (7) reads Y_{ijk} equals a constant source-type bias μ_i plus a random MDAC model inadequacy adjustment E_j plus a station noise adjustment $\epsilon_{(ij)k}$. The discriminant is formed from the difference of network (station averaged) values of P_g versus L_g, $\tilde{P}_g$ and $\tilde{L}_g$. Subtracting the historical average of this difference, when the seismic source is an explosion, and then dividing by the standard error gives a standardized difference

$$Z_{\bar{P}_g - \bar{L}_g} = \frac{(\bar{P}_g - \bar{L}_g) - \Delta_0}{\sqrt{\tau_{P_g}^2 + \sigma_{P_g}^2/n_{P_g} + \tau_{L_g}^2 + \sigma_{L_g}^2/n_{L_g}}}. \quad (18)$$

Applying the discriminant formulation Eq. (18) to the LLNL/LANL regional data gave $\Delta_0 = 0.43$, $\tau_{P_g}^2 = 0.23$, $\tau_{L_g}^2 = 0.16$, $\sigma_{P_g}^2 = 0.04$ and $\sigma_{L_g}^2 = 0.02$. P-values are shown in Figure 15. Regional phases are generated only by crustal events. Note that an interpretation of the P_g versus L_g P-value as evidence in
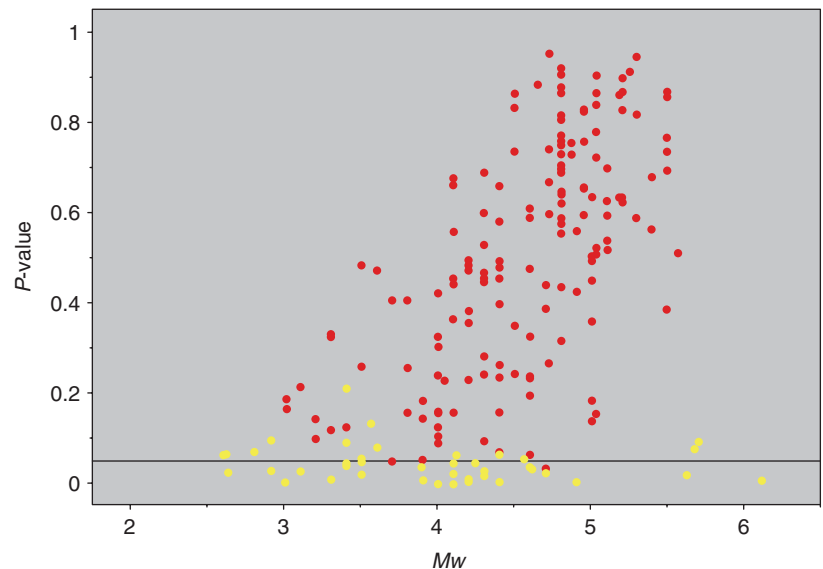
FIGURE 15 | P-values for the regional phase amplitude hypothesis $H_0 : \mu_{P_g} - \mu_{L_g} \geq 0.43$. Single-point fully contained explosions are shown in red, and shallow earthquakes are yellow.

support of $H_0 : \mu_{P_g} - \mu_{L_g} \geq 0.43$ leads to no missed explosions. Treating the P-value as a standardized discriminant, and choosing a decision line of approximately 0.05 also leads to no missed explosions.

INFRASOUND DISCRIMINANTS

From 1983 through September 1992 LANL operated infrasound arrays as part of a US Department of Energy program to detect the atmospheric acoustic signals generated by the surface ground motion of underground nuclear tests. The tests were performed at the Nevada Test Site, and the two permanent infrasound arrays at St. George, Utah (SG), and Los Alamos, New Mexico, operated continuously during this period. The physical process of the generation of infrasound from single-point fully contained explosions is a simple in concept. The strong, upward-directed, seismic wave from the explosion accelerates the surface and generates a signal in the atmosphere. With ground motion timescales of one to two seconds, signal frequencies would be around one Hertz. These low frequencies fall into the infrasonic (sub-audible) part of the acoustic spectrum. As with wave propagation in a variety of media, lower frequencies can propagate to longer ranges, making detection of these signals at regional distances possible.

The arrays used four low-frequency, high sensitivity microphones in a planar two-dimensional layout with inter-element spacings of 50–100 m, appropriate for the frequencies of interest. The data were digitized at 20 samples per second. Standard array processing software was used to process the data so that plane wave energy moving across the array would register as high correlation features. From the correlation analysis, the direction to the source (bearing or back azimuth) and trace velocity across the array are derived. For some events, temporary, portable arrays, were fielded whose characteristics were similar to the permanent arrays.

Because the arrays operated continuously, signals from other geophysical and man-made sources were recorded and analyzed as well. Three specific signal groups included explosive tests by the Department of Defense at White Sands Missile Range, earthquakes (southwest US and Mexico), and bolides (meteors). Earthquakes were of special interest because of ongoing research on seismic discriminants for earthquakes and fully contained single-point explosions. Earthquakes generate complex ground motion, and the vertical components can couple to the atmosphere, similar to the ground motion generated by fully contained single-point explosions.

Two preliminary infrasonic discriminants for separating earthquakes from single-point explosions include amplitude and duration. Peak surface accelerations are larger for single-point explosions due in part to differences in source physics: single-point explosions radiate compressional energy in all directions, whereas earthquake radiation is dependent upon the specific fault configuration. In addition, earthquakes typically occur deeper within Earth's crust than single-point explosions, thus a greater percentage of the seismic energy is dissipated by attenuation and geometrical spreading in the crust for comparable magnitude events. Earthquake ground motions last longer and encompass a larger area, resulting in longer duration signals from earthquakes in comparison to single-point explosions. Thus, signal duration is essentially a measure of source complexity and can be used to discriminate between relatively simple single-point explosion sources and more complex earthquake sources. Mutschlecner et al.[39] summarize infrasonic measurements and analysis for a number of earthquakes. Arrowsmith et al.[40] show that duration may be misleading in instances where ambient noise at the infrasound sensor is high, or where the event excites secondary sources of infrasound.

In contrast to the solid earth, the atmosphere is dynamic with medium motions (winds) reaching a significant fraction of the sound speed in the medium. This means that winds and gradients must be included in any wave propagation modeling. Energy from infrasound sources can propagate to large distances and in doing so can reach stratospheric and thermospheric heights (about 50 and 100 km, respectively). In an acoustic ray-tracing model, and for a source on the ground, energy moving along rays can be totally refracted at altitudes where the sound speed or sound speed plus wind speed in the direction of propagation exceeds the sound speed on the ground. In such cases one speaks of ducted propagation, and the ducts can be wind formed at stratospheric heights or due to temperature in the thermosphere. The winds in the stratosphere are seasonally dependent blowing to the east in the winter and west in the winter (in the northern hemisphere) and can affect the measured amplitudes of infrasound signals. These wind effects must be accounted for infrasonic amplitude for measurements during the year calculations. In effect one normalizes the amplitude to a zero stratospheric wind—a wind corrected amplitude (WCA).[41]

Similar to seismic signal propagation, waveform segments can be associated to different atmospheric paths and refraction altitudes, stratospheric and thermospheric phases. Stratospheric phases have average travel velocities between 0.28 and 0.31 km/s,
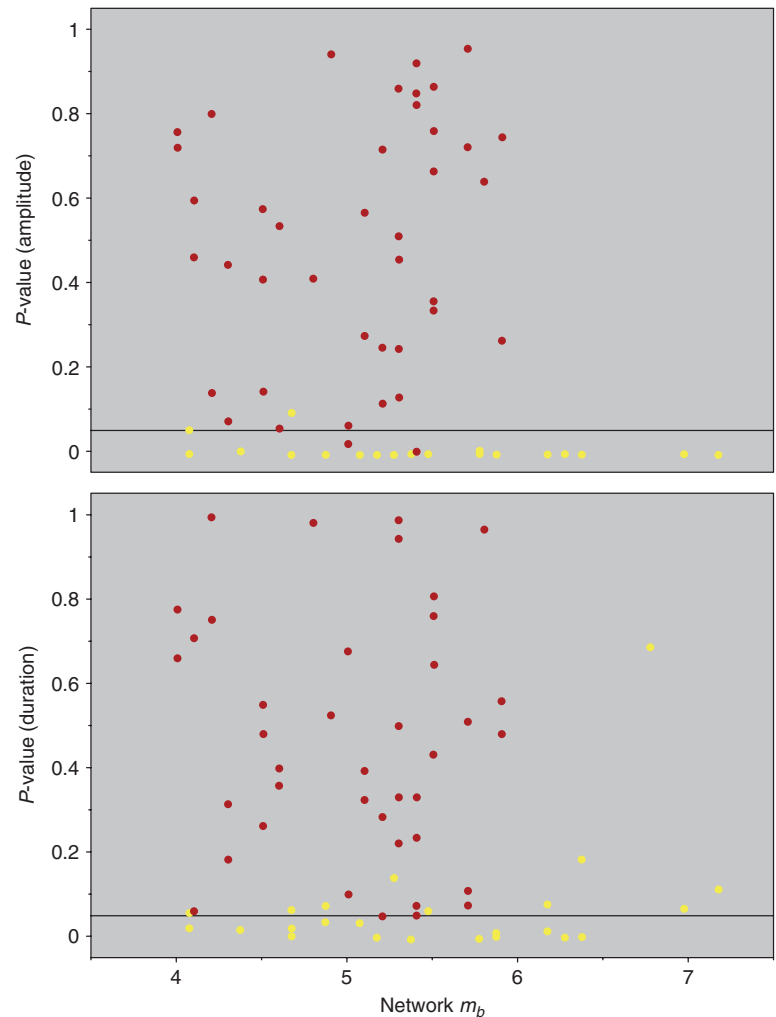
FIGURE 16 | Infrasound discriminant *P*-values for the conceptual null hypothesis H_0 : Single-point fully contained explosions. Explosions are shown in red, and shallow earthquakes are yellow.

and thermospheric phases are between 0.20 and 0.26 km/s. In addition, it is possible for tropospheric ducts to form due to wind or temperature structures and these phases would have average travel velocities larger than stratospheric values.

Events observed by the infrasound array SG are used to demonstrate the infrasound discriminants. In addition to the physical wind correction, a correction is necessary to remove confounding between source-type and event magnitude effects thus isolating source-type information. This correction is formulated as an analysis of covariance (ANCOVA) of log amplitude (or log duration) versus magnitude across source-types. ANCOVA source-type slopes are assumed equal and this model property has been validated with the St. George SG data. The usual ANCOVA assumptions have also been validated. Calibration data are used to develop the ANCOVA model. Residuals from the explosion component of the calibrated ANCOVA model can be used to develop a null hypothesis probability model, and the earthquake

residuals give the alternate hypothesis model. To identify an event, the calibrated explosion model is evaluated at the event magnitude, giving a prediction for the wind corrected discriminant and the residual. The residual is then used to calculate the *P*-value under the null hypothesis. Figure 16 shows *P*-values from the calibration analysis of the infrasound discriminants.

CONCLUSION

For a new seismic event, the process of characterization begins by constructing discriminants based on event-station distance. Historically, event discrimination has focused on teleseismic data, dictated by the size of the observed events, distribution of global stations, and simple paths traversed between events and stations. As global seismic station coverage has increased and the need to identify smaller events has grown in importance, regional observations become increasingly more important. For events that meet sufficient teleseismic signal-to-noise constraints at a

number of global stations, discriminants such as depth from hypocenter estimation, m_b-M_S, depth phases, first motion, and waveform complexity comprise separate tests that can be applied for event identification. Depth from hypocenter estimation assumes that single-point explosions can only occur at shallow depths which cannot exceed a certain threshold within drilling capability, while earthquakes can extend to many hundreds of kilometers depth. The m_b-M_S discriminant is based on the observation that single-point explosions have a lower M_S value than a shallow earthquake with a similar m_b; this discriminant can be complicated by the fact that deep earthquakes attenuate M_S and can appear explosion-like necessitating its use in tandem with a depth discriminant. The depth phase discriminant utilizes seismic depth phase arrivals seen in the waveforms to formulate a null hypothesis in two ways (composite simple linear regression and an order statistics based model). First motions are used to classify the initial earth movement of an event; regardless of the location of the seismometer, first motions for explosions should be upward (positive), while earthquakes will have a mixture due to the nature of fault rupture. Waveform complexity takes advantage of the observation that shallow earthquakes are fundamentally more complex with respect to P-waves as opposed to single-point explosions, and associated P-values from complexity measurements are extremely successful, leading to no missed explosions and no false alarms.

With the modern drive toward regional discrimination, phase amplitude and infrasound discrimination provide multisensor signatures for enhanced discrimination. The phase amplitude discriminant is formulated in a similar way to m_b-M_S, although consideration for complex propagation paths must be accounted for at regional distances prior to forming discriminants. Infrasound data represent a unique and useful method for detecting surface and near-surface events. Initial results show good separation of event classes, suggesting the utility of non-seismic measurements for event identification. For the datasets used in this article, we have demonstrated the high degree of success in separation of earthquake and explosion populations. For any given discriminant, the success rate performance is not perfect, motivating the need to combine discriminants. Future research should fundamentally focus on the construction of the discriminants rather than technologies to combine discriminants, as there are many mature technologies for multivariate discrimination (see Ref 42). For discriminant research the fundamental challenge is the mathematical combination of physical basis with probability models to describe sources of error. The criteria for selection of a multivariate discrimination technology is operational utility and relevance.

REFERENCES

1. Andryushin IA, Voloshin NP, Ilkaev RI, Matushchenko AM, Ryabev LD, Strakov VG, Cherryshev AK, Yudin Yu A. *Catalog of Worldwide Nuclear Testing*. Mikhailov VN, ed.; Begell-Atom, New York; 1999.

2. Bolt B. *Nuclear Explosions and Earthquakes: The Parted Veil*. San Francisco: W. H. Freeman and Company; 1976.

3. Dahlman O, Israelson H. *Monitoring Underground Nuclear Explosions*. Amsterdam: Elsevier Science, North Holland; 1977.

4. Bates CC. VELA UNIFORM, the nation's quest for better detection of underground nuclear explosions. *Geophysics* 1961, 26:499–507.

5. Stauder W, Bolinger GA. The s-wave project for focal mehcnism studies, earthquakes of 1963. *Bull Seismol Soc Am* 1963, 56:1363–1371.

6. Cooley JW, Tukey JW. An algorithm for the machine calculation of complex Fourier series. *Math Comput Model* 1965, 19:297–301.

7. Anderson DN, Fagan DK, Tinker MA, Kraft GD, Hutchenson KD. A mathematical statistics formulation of the teleseismic explosion identification problem with multiple discriminants. *Bull Seismol Soc Am* 2007, 97:1730–1741.

8. Anderson DN, Walter WR, Fagan DK, Mercier TM, Taylor SR. Regional multi-station discriminants: magnitude, distance and amplitude corrections and sources of error. *Bull Seismol Soc Am* 2009, 99: 794–808.

9. Blandford RR. Discrimination between earthquakes and underground explosions. *Ann Rev Earth Planetary Sci* 1977, 5:111–122.

10. Douglas, A. (1981). Seismic source identification: a review of past and present research efforts. In Husebye E, Mykkeltveit S, eds. *Identification of Seismic Sources–Earthquake or Underground Explosion*, pages 1–48. D. Reidel Publishing Co., Dordrecht, The Netherlands.

11. Douglas A. Forensic seismology revisited. *Surv Geophys* 2007, 28:1–31.

12. Mueller RA, Murphy JR. Seismic characteristics of underground nuclear detonations: part I. Seismic spectrum scaling. *Bull Seismol Soc Am* 1971, 61: 1675–1692.

13. Murphy JR, Mueller RA. Seismic characteristics of underground nuclear detonations: part II. Elastic energy and magnitude determinations. *Bull Seismol Soc Am* 1971, 61:1693–1704.

14. Patton HJ, Taylor SR. Effects of shock-induced tensile failure on m_b-M_S discrimination: contrasts between historic nuclear explosions and the North Korean test of 9 October 2006. *Geophys Res Lett* 2008, 35:L14301.

15. Bonner JL, Russell DR, Harkrider DG, Reiter DT, Herrmann RB. Development of a time-domain, variable-period surface-wave magnitude measurement procedure for application at regional and teleseismic distances: Part II: Application and $M_s - m_b$ performance. *Bull Seismol Soc Am* 2006, 96:678–696.

16. Seber GAF, Wild CJ. *Nonlinear Regression*. New York: John Wiley & Sons; 1989.

17. Marshall PD, Basham PW. Discrimination between earthquakes and underground explosions employing an improved M_S scale. *Geophys J R Astron Soc* 1972, 29:431–458.

18. Evernden JF. Further studies on seismic discrimination. *Bull Seismol Soc Am* 1975, 65:359–391.

19. Blandford RR. Seismic event discrimination. *Bull Seismol Soc Am* 1982, 72:69–87.

20. Stevens JL, Day SM. The physical basis of the m_b:M_S and variable frequency magnitude methods for earthquake/explosion discrimination. *J Geophys Res* 1985, 90:3009–3020.

21. Kennett BLN, Engdahl R. Travel times for global earthquake location and phase identification. *Geophys J Int* 1991, 105:427–465.

22. Kennett BLN. (1991), *IASPEI 1991 seismological tables*. Technical report, Research Shcool of Earth Sciences, Australia National University, Canberra.

23. Kraft GD. (1999), *An improved method for determining pP-P stepout*. Technical Report ARS-99-028, ENSCO, Inc., Melbourne, Florida.

24. Taylor SR, Anderson DN. Rediscovering signal complexity as a teleseismic discriminant. *Pure Appl Geophys* 2009, 999:1–13.

25. Koch K, Schlittenhardt J. The use of teleseismic P-wave complexity for seismic event screening—results determined from GRF and GERESS array data. *J Seismol* 2002, 6:183–197.

26. Ortiz AM, Taylor SR, Fitzgerald TJ, and Wallace T (2002), *Rediscovering signal complexity discriminants: A preliminary study for application to regional seismic and radio frequency signatures*. Technical Report LAUR-02-7657, Los Alamos National Laboratory, Los Alamos, New Mexico.

27. Douglas A, Marshall PD, Gibbs PG, Young JB, Blamey C. P signal complexity re-examined. *Geophys J R Astron Soc* 1973, 33:195–221.

28. Douglas A, Young JB, Hudson JA. Complex P-wave seismograms from simple earthquake sources. *Geophys J R Astron Soc* 1974, 37:141–150.

29. Barley BJ. The origin of complexity in some P seismograms from deep earthquakes. *Geophys J R Astron Soc* 1977, 49:773–777.

30. Bowers D. On the probability of mistaking an earthquake for an explosion using the simplicity of P. *Bull Seismol Soc Am* 1996, 86:1925–1934.

31. McLachlan GJ. *Discriminant Analysis and Statistical Pattern Recognition*. New York: John Wiley & Sons; 1992.

32. Pomeroy PW, Best WJ, McEvilly TV. Test ban treaty verification with regional data—a review. *Bull Seismol Soc Am* 1982, 72:S89–S129.

33. Taylor SR, Hartse HE. A procedure for estimation of source and propagation amplitude corrections for regional seismic discriminants. *J Geophys Res* 1998, 103:2781–2789.

34. Taylor SR, Velasco AA, Hartse HE, Phillips WS, Walter WR, Rodgers AJ. Amplitude corrections for regional seismic discriminants. *Pure Appl Geophys* 2002, 159:623–650.

35. Walter WR and Taylor SR (2002), *A revised magnitude and distance amplitude correction (MDAC2) procedure for regional seismic discriminants: Theory and testing at NTS*. Technical Report LAUR-02-1008, Los Alamos National Laboratory, Los Alamos, New Mexico.

36. Walter WR, Mayeda K, Patton HJ. Phase and spectral ratio discrimination between NTS earthquakes and

explosions: part 1: empirical observations. *Bull Seismol Soc Am* 1995, 85:1050–1067.

37. Taylor SR. Analysis of high-frequency Pg/Lg ratios from NTS explosions and western U.S. earthquakes. *Bull Seismol Soc Am* 1996, 86:1042–1053.

38. Bottone S, Fisk MD, McCartor GD. Regional seismic-event characterization using a bayesian formulation of simple kriging. *Bull Seismol Soc Am* 2002, 92:2277–2296.

39. Mutschlecner JP, Whitaker RW. Infrasound from earthquakes. *J Geophys Res* 2005, 110:1–11.

40. Arrowsmith SJ, Burlacu R, Whitaker RW, Randall GE. A repeating secondary source of infrasound from the Wells, Nevada earthquake sequence. *Geophys Res Lett* 2009, 36:L11817, doi: 10.1029/2009GL038363.

41. Mutschlecner JP, Whitaker RW, and Auer LH (1999), *An empirical study of infrasound propagation*. Technical Report LA-13620-MS, Los Alamos National Laboratory, Los Alamos, New Mexico.

42. Hand DJ. Classifier technology and the illusion of progress. *Stat Sci* 2006, 21:1–34.